

Influence of substitutional disorder on the electrical transport and the superconducting properties of $\text{Fe}_{1+z}\text{Te}_{1-x-y}\text{Se}_x\text{S}_y$

M. G. Rodríguez ^{1a}, G. Polla^b, C. P. Ramos^b, C. Acha ^{2a}

^a*Laboratorio de Bajas Temperaturas, Departamento de Física, FCEyN, UBA and IFIBA-CONICET, Buenos Aires, Argentina*

^b*Gerencia de Investigación y Aplicaciones, CAC-CNEA, San Martín, Argentina*

Abstract

We have carried out an investigation of the structural, magnetic, transport and superconducting properties of $\text{Fe}_{1+z}\text{Te}_{1-x-y}\text{Se}_x\text{S}_y$ ceramic compounds, for $z = 0$ and some specific Se ($0 \leq x \leq 0.5$) and S ($0 \leq y \leq 0.12$) contents. The incorporation of Se and S to the FeTe structure produces a progressive reduction of the crystallographic parameters as well as different degrees of structural disorder associated with the differences of the ionic radius of the substituting cations. In the present study, we measure transport properties of this family of compounds and we show the direct influence of disorder in the normal and superconductor states. We notice that the structural disorder correlates with a variable range hopping conducting regime observed at temperatures $T > 200$ K. At lower temperatures, all the samples except the one with the highest degree of disorder show a crossover to a metallic-like regime, probably related to the transport of resilient-quasi-

¹Scholarship from CONICET of Argentina

²Corresponding author: acha@df.uba.ar

particles associated with the proximity of a Fermi liquid state at temperatures below the superconducting transition. Moreover, the superconducting properties are depressed only for that particular sample, in accordance to the condition that superconductivity is affected by disorder when the electronic localization length ξ_L becomes smaller than the coherence length ξ_{SC} .

Keywords:

Superconductivity, Fe-based superconductors, electrical transport, disorder

1. Introduction

Since the discovery of superconductivity in the iron pnictide system [1], ReFeAsO (Re: rare earth) doped by chemical substitution on the Re or in the O site [2, 3], at temperatures between 40 K and 55 K and with critical fields of 65 T at 4 K, a large quantity of studies was devoted to these Fe-based superconductors. Among them, it was shown [4] the existence of a related family of superconductors, the iron chalcogenides, corresponding to FeSe and FeTe and their partial substitutions $\text{FeTe}_{1-x}\text{Se}_x$. This system has the simplest structure among the Fe-based superconductors because it is formed just with two layers of Fe and Se/Te, with an anti-PbO structure (space group $P4/nmm$) [5].

The FeTe compound exhibits antiferromagnetic (AF) ordering below $T_N \sim 70$ K and no superconducting state [6] down to 4 K. By partial substitution of Te by Se or by S, the AF order is suppressed and superconductivity develops [7, 8] at critical temperatures $T_c \sim 8$ K - 14 K. On the other hand, FeSe is a superconductor and the partial substitution of Se by S initially favors superconductivity, while for replacements over a 20% superconductiv-

ity is depressed [9]. Up to now, studies of the influence of disorder on the properties of iron chalcogenides were particularly devoted to substitutions into the Fe-site [10, 11]. Here, in order to gain insight on the influence of structural parameters on the normal state properties and on the appearance of the superconducting state on these Fe-based chalcogenide superconductors, we have synthesized new ceramic samples, performing partial substitutions of Te in the FeTe compound by both Se and S, corresponding to $\text{Fe}_{1+z}\text{Te}_{1-x-y}\text{Se}_x\text{S}_y$ (FTSeS). The Se and S concentrations were chosen in order to maintain nearly constant the ionic radius while producing a small increase of the structural disorder in the chalcogenide site.

In the present work, we particularly report on the synthesis and structural characterization of the FTSeS ceramic samples and on their magnetic, transport and superconducting properties. We found that the structural disorder of the chalcogenide site (σ) influences the transport properties, determining a 3D-variable range hopping conduction-regime observed for temperatures $T > 200$ K, with an electronic localization length (ξ_L) that decreases concomitantly with increasing σ . We found a marked reduction of T_c for the sample where ξ_L becomes lower than the coherence length (ξ_{SC}), indicating the sensibility of the superconducting state to nonmagnetic disorder.

2. Experimental Details

We have synthesized, by solid-state reaction, the family of FTSeS ceramics compounds, with nominal compositions $z=0$ and $(x, y) = (0, 0.12); (0.10, 0.10); (0.25, 0.06); (0.30, 0.05); (0.40, 0.02); (0.45, 0.01)$ and $(0.50, 0)$. The x and y values were chosen in order to produce a small variation of the av-

average chalcogenide ionic radius ($\langle R_{Ch} \rangle = \sum x_i R_i$, where the x_i are the fractional occupancies of each chalcogenide and R_i their ionic radius) while increasing the random disorder associated with their different ionic radius. To vary this disorder, we use different Te, Se and S combinations in order to modify the standard deviation $\sigma = \sqrt{(\sum x_i R_i^2 - \langle R_{Ch} \rangle^2)}$ and $\langle R_{Ch} \rangle$ was chosen around (2.12 ± 0.04) Å. As the starting materials, we used high-purity elements, Fe, Te, Se and S (Alfa Caesar 99.99 %). Considering their increasing Se contents these samples were labeled S01 to S07, respectively. The materials were ground, pelletized and encapsulated in a quartz tube in vacuum. Then, the samples were heated at 750 °C for over 24 hours and slowly cooled down to room temperature. We repeated the heat treatments again and finally, we resintered the samples in a rectangular shape at 750 °C but reducing time to 12 hours.

Samples were characterized by x-ray powder diffraction (XRD) using a CuK α radiation with a PANalytical Empyrean model diffractometer with PIXcel 3D detector. A complete Rietveld refinement was done with Full Prof program [12]. Mössbauer spectra of the S07 sample were obtained at room temperature (RT) and 20 K with a conventional constant acceleration spectrometer in transmission geometry with a $^{57}\text{Co}/\text{Rh}$ source. Measurements were recorded at 4 mm/s and 11 mm/s and then fitted using the Normos program [13]. Isomer shift values are given relative to that of α -Fe at RT. A quantitative point analysis was performed by energy dispersive x-ray spectroscopy (EDX) coupled with a scanning electron microscopy (SEM). All the samples were polished before the measurements. We made several measurements on the whole surface and then we averaged to obtain a more

realistic value of content of each sample. Electrical resistivity measurements as a function of temperature ($4 \text{ K} \leq T \leq 300\text{K}$) were performed by a four-point method. Magnetization as a function of temperature and hysteresis loops were achieved using a squid magnetometer.

3. Results and Discussion

A typical XRD pattern obtained in this case for sample S07 and its Rietveld refinement can be observed in Fig. 1. Similar results were obtained for the whole batch of FTSeS samples. The refinements were performed by considering a tetragonal structure $P4/nmm$. The presence of a fraction less than $\sim 8\%$ of Fe_7Se_8 as impurity was also refined for all the samples. Peaks associated with this impurity were marked with an asterisk in Fig. 1.

For a more detailed characterization of sample S07, a Mössbauer spectrum was recorded at room temperature (RT) and 11 mm/s (not shown here). A dominant broad doublet showed up and a minor content of impurity magnetic phases seemed to be hidden in the background. In order to allow a better resolution of the paramagnetic hyperfine splitting, an additional spectrum was recorded at 4 mm/s, in which two main paramagnetic components are clearly distinguished (Fig. 2a). The major one has an isomer shift of 0.45 mm/s and a quadrupole splitting of 0.28 mm/s, in coincidence with the hyperfine parameters reported in literature for $\text{FeTe}_{0.5}\text{Se}_{0.5}$ [14, 15]. The other one instead has an isomer shift of 0.26 mm/s and a quadrupole splitting of 0.78 mm/s. This last subspectrum with Fe^{3+} character could be due to a superparamagnetic contribution of impurity phases with particle sizes typically smaller than 10 nm. Those parameters were then fixed in

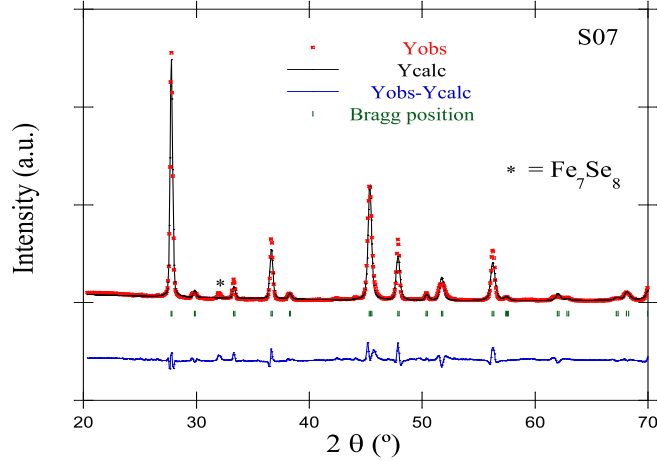


Figure 1: (Color online) XRD patterns for sample S07 (red squares) and its Rietveld refinement (black line). Differences and the Bragg position of the reflexions correspond to blue lines and to green vertical lines, correspondingly. The presence of the Fe_7Se_8 impurity is also indicated.

the spectrum recorded at RT and 11 mm/s, to take into account only the minor magnetic component. For that purpose a fitting with a hyperfine field distribution for the higher fields (> 10 T) was performed (see Fig. 2b).

This analysis revealed the presence of at least two impurity phases. An appropriate identification required another spectrum recorded at low temperature and 11 mm/s. In this case, to ensure a temperature below any possible transition, 20 K was chosen. The corresponding hyperfine field distribution is also shown in Fig. 2b. The area under the magnetic part of the spectrum slightly increased when lowering temperature, confirming that as it was supposed above in the text, the minor doublet contribution at RT arose from superparamagnetic impurities. Based on the whole analysis, in-

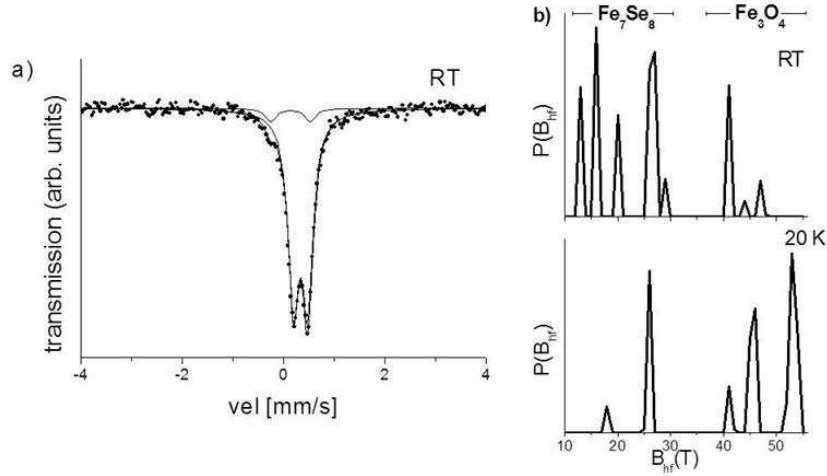


Figure 2: a) Mössbauer spectrum of $FeTe_{0.5}Se_{0.5}$ in a narrow velocity range at RT, including paramagnetic components fitting, b) Hyperfine field distributions at RT and 20 K for the magnetically ordered contributions.

cluding RT measurements in wide and narrow velocity ranges and at low temperature, it can be concluded that one of the impurity phases is magnetite (Fe_3O_4); distinguished on cooling due to the Verwey transition [21]. Considering the recoilless factor of Fe_3O_4 at RT, reported in [15], the effective fraction of magnetite in the sample would not exceed 3%. The other one, a low field contribution to the hyperfine distribution at RT which evolves to higher fields as lowering temperature, would agree with the spin reorientation corresponding to Fe_7Se_8 . [22] This impurity fraction represents about 10% of

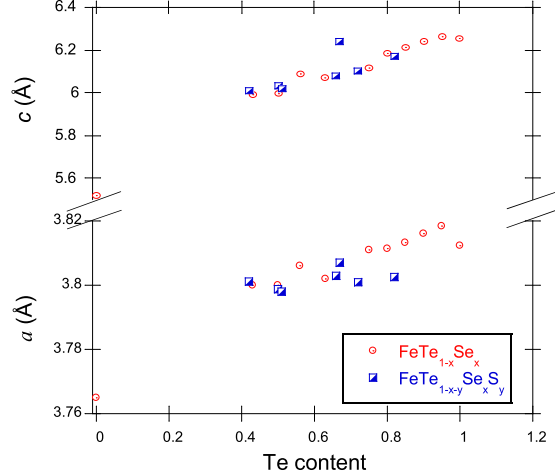


Figure 3: (Color online) Crystallographic parameters a and c as a function of the real Te content for the FTSeS samples. Data for the $\text{FeTe}_{1-x}\text{Se}_x$ (FTSe) samples is also included for comparison (from ref. [16, 7, 17, 18, 19, 20])

the iron bearing compounds in the sample. These results do not contradict the XRD measurements in which Fe_7Se_8 with a similar fraction was detected. Fe_3O_4 was not distinguished due to the experimental resolution of the XRD technique (a phase fraction lower than 5% is difficult to detect).

The evolution of both a and c crystallographic parameters by increasing the substitution of Te by Se or S can be observed in Fig. 3. Our results are compared with those corresponding to the Te substitution by Se for the $\text{FeTe}_{1-x}\text{Se}_x$ (FTSe) compound. It can be observed that mainly the a and c parameters are reduced when decreasing the Te content of the sample, similarly to the results observed for the FTSe samples. Although some exceptions can be noted (like an anomalous high value of the c parameter for sample S03) that can be associated with an excess of Fe, probably occupying

Table 1: Composition determined by EDX (± 0.02 for Te, Se and S and ± 0.04 for Fe), standard deviation of the radius of the chalcogenide site σ ($\pm 5\%$), crystallographic a and c parameters, superconducting transition temperature defined by magnetization and transport measurements ($\pm 3\%$), coefficient T_0 (see Eq. 2, $\pm 8\%$) and localization length ξ_L ($\pm 3\%$).

Sample	EDX composition	σ (Å)	a (Å)	c (Å)	T_c^{mag} (K)	T_c^{res} (K)	T_0 (K)	ξ_L (Å)
S01	Fe _{1.15} Te _{0.72} S _{0.28}	0.166	3.800(9)	6.10(4)	-	6.8	2294	1.8
S02	Fe _{0.88} Te _{0.82} Se _{0.09} S _{0.09}	0.119	3.802(5)	6.16(9)	6.6	9.9	403	3.3
S03	Fe _{1.25} Te _{0.67} Se _{0.27} S _{0.06}	0.125	3.807(0)	6.23(8)	11.3	12.3	853	2.5
S04	Fe _{1.18} Te _{0.66} Se _{0.28} S _{0.06}	0.125	3.802(9)	6.08(1)	12.2	13.0	435	3.2
S05	Fe _{0.92} Te _{0.50} Se _{0.46} S _{0.04}	0.123	3.798(7)	6.03(4)	13.1	13.5	337	3.5
S06	Fe _{1.13} Te _{0.51} Se _{0.47} S _{0.02}	0.120	3.798(0)	6.01(7)	13.3	13.5	297	3.6
S07	Fe _{0.99} Te _{0.42} Se _{0.58}	0.114	3.801(1)	6.00(8)	14.3	14.0	524	3.0

interstitial sites. [23]

The real composition of the samples was estimated by the semi-quantitative determination of an EDX analysis. Five to seven points were chosen on the surface of the sample in order to get an average composition. A typical dispersion of 0.02 was obtained for Te, Se and S, and was slightly higher for Fe (0.04). This higher value can be related to the presence and distribution of Fe-based impurities, which may also produce an overestimation of the Fe content. Results obtained by Rietveld refinements and by EDX analysis are summarized in Table 1.

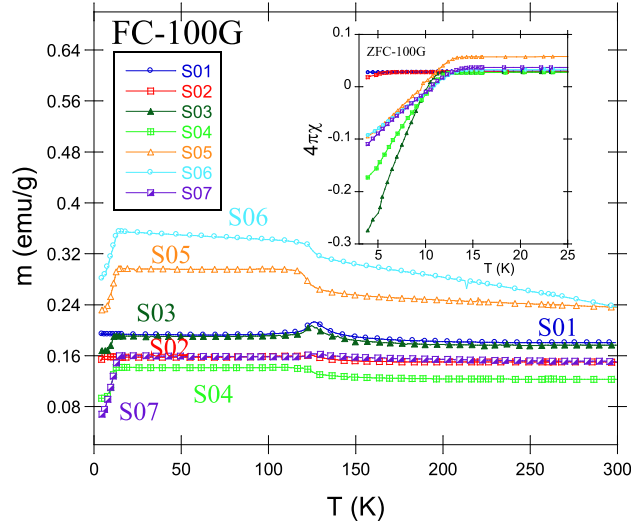


Figure 4: (Color online) FC magnetization as a function of temperature for samples S01 to S07 at 100 G. The inset shows the ZFC DC susceptibility ($4\pi\chi$) as a function of temperature. T_c can be defined by the position of the onset of the diamagnetic signal.

Field-cooled (FC) magnetization measurements as a function of temperature at 100 G for samples S01 to S07 are shown in Fig. 4. The superconducting transitions for samples S02 to S07 can be observed at low temperatures while a ferromagnetic background is also present for all the samples with an anomalous cusp around 125 K. The inset of Fig. 4 shows the 100 G zero-field-cooled (ZFC) DC susceptibility measurements ($4\pi\chi$) at low temperatures, which gives a rough idea of the superconducting volume fraction. The onset and the width of the superconducting transitions for samples S02 to S07 can be observed, where the absence of a magnetic shielding for sample S01 can be confirmed. Sample S02 also shows a very small diamagnetic signal, indicating that superconductivity develops only in a minority phase. The other samples show a higher superconducting response, although complete

bulk superconductivity is not achieved. T_c was defined as the onset of this signal and reported in Table 1 as T_c^{mag} .

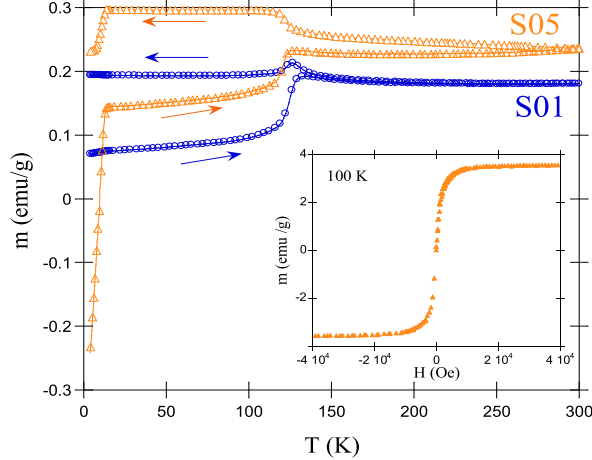


Figure 5: (Color online) FC and ZFC magnetization (100 G) as a function of temperature for samples S01 and S05. The observed cusp at $T \simeq 125$ K (Verwey transition) and the low temperature irreversibilities are characteristic of the presence of Fe_3O_4 . The inset shows the isothermal magnetization $M(H)$ of sample S05 at 100 K.

Fig. 5 shows the FC and the ZFC magnetization curves for samples S01 and S05. Similar results were obtained for the other FTSeS samples. The cusp observed around 125 K is the clear signature of the Verwey transition [21] associated with the presence of minor phase Fe_3O_4 . In fact, most of the magnetization of the normal state can be related to the Fe_7Se_8 and Fe_3O_4 impurities [20, 24], as the ferromagnetic background and the hysteretic behavior depicted for temperatures $T > 130\text{K}$ is also typical of Fe_7Se_8 , or of Fe_3O_4 grains with nanometric dimensions [25, 26]. The magnetization curve M vs H at $T=100$ K showed in the inset of Fig. 5 corresponding to sample

S05 (although this curve was practically sample and temperature independent in the 50 K to 300 K range) is characteristic of Fe_3O_4 . By considering its saturation value (3.4 emu/g) we estimate the presence of $\sim 4\%$ in mass of this impurity [27], in accordance with the Mössbauer spectrum.

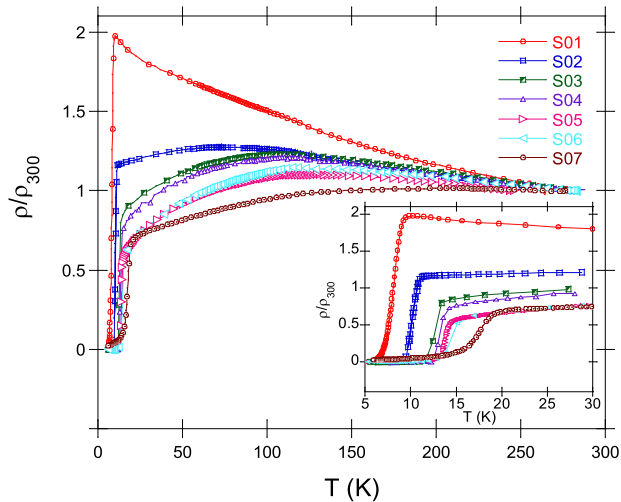


Figure 6: (Color online) Temperature dependence of the normalized resistivity ($\rho/\rho_{(300K)}$) for samples S01 to S07. The inset shows the detail of the resistive superconducting transition for samples S01 to S07.

The normalized resistivity ($\rho/\rho_{(300K)}$) as a function of temperature is shown in Fig. 6. A semiconducting-like behavior at temperatures $T > 150$ K can be observed for all the samples while, for samples S02 to S07, a hump and a metallic-like conduction is obtained with further decreasing temperature. Only sample S01 remains as an insulator down to its superconducting transition. This particular metallic-like conduction observed at low temperatures, with an increasing slope with decreasing temperature, is characteristic of many Fe-chalcogenide superconductors. [28] This non-Fermi-Liquid

(NFL) behavior was recently associated with a resilient quasi-particle (RQP) regime [29], where the resistivity is still dominated by FL quasi-particles, in an intermediate temperature range, between a FL and a bad metal phase.

In the RQP regime, resistivity is not following the T^2 dependence expected for a FL, nor the linear behavior of a bad metal. This latter regime is attained when the resistivity reaches the Mott Ioffe Regel limit (ρ_{MIR}). [30] Until that point, resistivity evolves in the RQP regime, showing a negative intercept and a gradual tendency to a linear regime as the temperature is increased well above the FL transition temperature.

To check if the observed anomalous metallic-like behavior at low temperatures (Fig. 6) is developed between these limits, a rough estimation of ρ_{MIR} can be obtained, assuming a spherical Fermi surface and a carrier density of $10^{20} - 6 \times 10^{20} \text{ cm}^{-3}$. [31] This gives $\rho_{MIR} \simeq 2\text{-}6 \text{ m}\Omega \text{ cm}$. As the resistivities of our FTSeS samples (0.2 to 0.4 $\text{m}\Omega \text{ cm}$) are well below ρ_{MIR} , it is consistent to consider that the observed NFL behavior develops in a RQP regime.

Unlike what we observed in magnetic measurements, impurities have a negligible contribution to resistivity. This fact is indeed clear as at the Verwey transition ($\simeq 125 \text{ K}$) the resistivity of Fe_3O_4 diverges, but no appreciable changes are observed in our resistivity curves (see Fig. 6).

The inset of Fig. 6 shows the detail of the superconducting transitions, present for all the samples, even for sample S01, indicating in this case its filamentary nature, as no superconducting shielding was noticed in the magnetization measurements down to 4 K (see Fig. 4). We would like to note here that S01 and S02 samples are those that show a highly depressed superconducting state ($T_c < 10 \text{ K}$, with a superconducting volume $< 1\%$), while

samples S03 to S07 present a more robust superconducting phase. We define the superconducting transition temperature (T_c) as the temperature where the superconducting state percolates ($\rho \rightarrow 0$) and we reported this value in Table 1 as T_c^{res} .

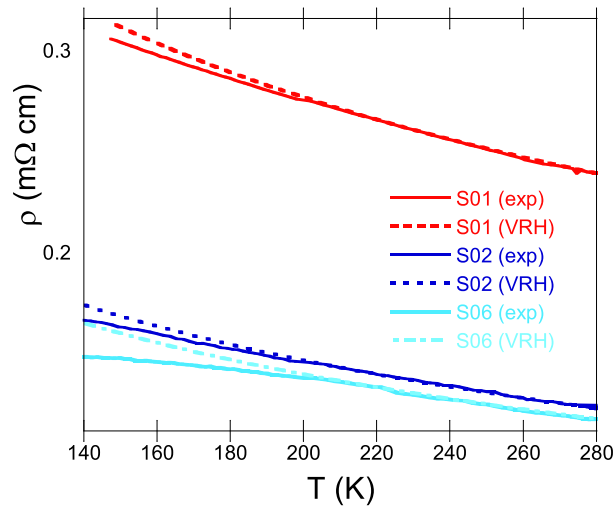


Figure 7: (Color online) Temperature dependence of resistivity for samples S01, S02 and S06. A VRH law gives the best fit of data for temperatures $T > 200K$. Experimental data deviates from the VRH law for $T \leq 200$ K.

We have particularly analyzed the semiconducting-like conduction regime for the FTSeS samples ($150 \text{ K} \leq T \leq 300 \text{ K}$). To fit the temperature dependence of the resistivity, we propose a general expression of the form:

$$\rho = \rho_0 \exp[(T_0/T)^n], \quad (1)$$

in order to determine if the conduction regime corresponds to a semiconductor or to a disordered metal. In the first case, T_0 is associated with the band

gap, while in the second case, it is related to the electronic localization length ξ_L , with T_0 increasing with increasing disorder [32], as expressed in Eq. 2.

$$T_0 \simeq \left\{ \frac{21.2}{k_B N(E_f) \xi_L^3} \right\}, \quad (2)$$

where k_B is the Boltzman constant and $N(E_f)$ the density of states at the Fermi energy.

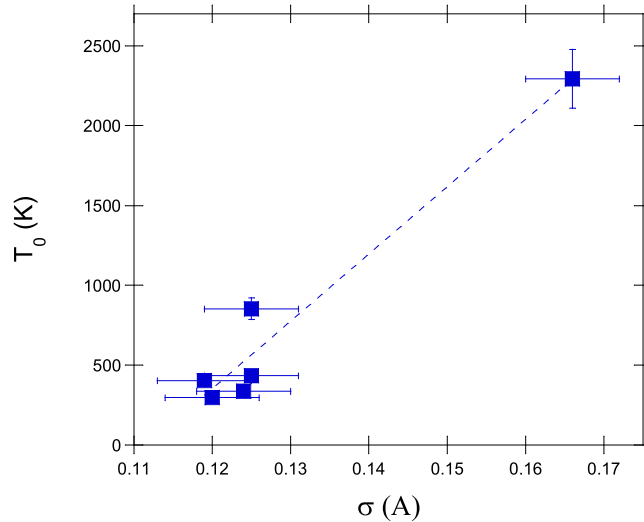


Figure 8: (Color online) T_0 parameter (see Eq. 2) as a function of the structural degree of disorder σ .

We found that the best fit is obtained for $n=0.25 \pm 0.02$, which agrees with a variable range hopping (VRH) law, indicating that disorder is determining the electrical conduction of the FTSeS samples for $T > 200$ K. Fig. 7 shows the results of these fits for samples S01, S02 and S06. Similar results were obtained for the other samples. The experimental data is compared with the VRH law, showing that our samples present an excess conductivity to the one expected for the VRH law for temperatures $T < 200$ K. These

deviations from the high temperature VRH conduction may be associated to a crossover to another conducting regime, particularly to the RQP mentioned previously. The RQP regime would dominate the electrical transport at low temperatures, with an scattering probably associated with incoherent charge dynamics for samples S02 to S07. The low temperature resistivity of sample S01 could not be fitted by a VRH or a semiconductor temperature dependence. It is clear that the RQP regime is not developed as for samples S02 to S07, but it may produce an additional conduction that impedes to describe the temperature dependence of its resistivity with a simple expression.

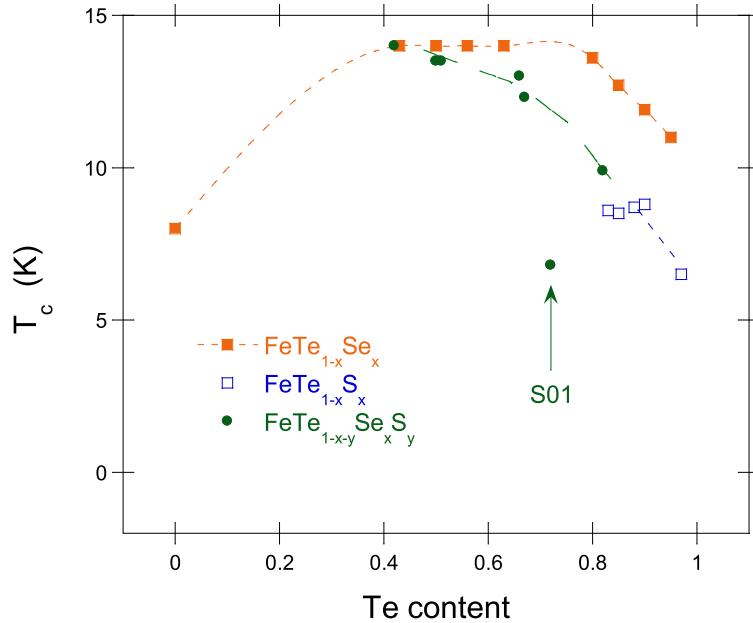


Figure 9: (Color online) T_c as a function of the Te content for the family $\text{FeTe}_{1-x}\text{Se}_x$ (FTSe) [16, 33, 34, 17], $\text{FeTe}_{1-x}\text{S}_x$ (FTS) [35] and FTSeS (our work). The data point of the S01 sample is indicated with an arrow. Lines are a guides to the eye.

A similar low temperature localization-like regime, with a filamentary

superconducting state was also observed for samples with high Te content and also extended for lower Te contents by increasing the interstitial Fe in excess. [36] Their electrical transport source of scattering was associated with dynamic magnetic correlations with in plane magnetic wave vector $(\pi,0)$, considered antagonistic to superconductivity.

In Fig. 8 we have plotted the fitted T_0 parameter from the VRH conduction model (see Eq. 1) as a function of the standard deviation of the chalcogenide radius σ . Although the distribution of σ values is not uniform in the explored range, due to the fact that the measured composition differs from the programmed nominally, the tendency that T_0 increases with increasing σ can be conjectured, suggesting that the structural disorder introduced by substitutions in the chalcogenide site may be the main source of disorder that controls the electrical conduction of the normal state.

In order to gain insight in which is the influence of the structural disorder on the superconducting state, we show in Fig. 9 the Te content dependence of T_c^{res} for the families $\text{FeTe}_{1-x}\text{Se}_x$ (FTSe), $\text{FeTe}_{1-x}\text{S}_x$ (FTS) and FTSeS (our work). It can be observed that the FTSeS samples have an intermediate T_c between the FTSe and FTS families. Surprisingly, the T_c of sample S01 is highly depressed in comparison to the others, clearly out of the general behavior, although its Te content is not the highest. Its Fe content is also high but it is even lower than the one of sample S03 which has a higher T_c . As this is the sample with the highest σ , we may consider if its weaker and filamentary superconducting state could be a consequence of its strongly electronic localization. In a simple approach, the superconducting T_c would be depressed when the localization length (ξ_L) is lower than its superconduct-

ing coherence length (ξ_{SC}). [37] To verify this possibility, a value of $\xi_{SC} \simeq 2.5$ nm was estimated from upper critical field (H_{c2}) measurements [38] by assuming a 3D-Ginzburg-Landau relation. The ξ_L of samples FTSeS (see Table 1) can be obtained from Eq. 2 by considering a cell volume $V_c \simeq 85 \text{ \AA}^3$, $N(E_f) \simeq 2\text{States}/eV/V_c$ [39] and the temperatures T_0 obtained by fitting the VRH conduction for $T \geq 200$ K. For sample S01, ξ_L (1.8 nm) is lower than ξ_{SC} , while it is not the case for all the other samples (S02 to S07), in accordance to the assumption that disorder is affecting its superconducting state.

4. Conclusions

To summarize, we have synthesized a new family of superconducting samples with different degrees of disorder on the chalcogenide site by partially replacing Te by both Se and S in the FeTe compound. We determined that magnetic properties in the normal state are dominated by the presence of small amounts ($\simeq 3\text{-}4\%$) of Fe_3O_4 and ($\simeq 8\text{-}9\%$) Fe_7Se_8 , while their influence on electrical transport properties is negligible. These usual impurities obtained in the synthesis of the FTSe compound [14, 26] produce a ferromagnetic background, an anomaly near 125 K, corresponding to the Verwey transition of magnetite, and an hysteretic behavior in the 150 K to 300 K range probably associated with the ferrimagnetic nature of Fe_7Se_8 . The AF order, present for the FeTe compound, was not detected for the range of the substitutions explored. We have shown that disorder on the chalcogenide site (estimated by the parameter σ) influences the electrical resistivity for temperatures higher than 200 K, determining a VRH conduction regime for

all the samples. A metallic-like conduction, with characteristics of a RQP regime, develops at lower temperatures for all the samples except for the one with the highest degree of disorder (S01). Particularly for this sample, superconductivity is highly depressed as expected when disorder reduces the electronic localization length below the superconducting coherence length.

5. Acknowledgments

We would like to acknowledge financial support by CONICET Grant PIP 112-200801-00930 and UBACyT 20020100100679 (2011-2014). We also acknowledge V. Bekeris for a critical reading, and D. Giménez, E. Pérez Wodtke and D. Rodríguez Melgarejo for their technical assistance.

6. References

References

- [1] Y. Kamihara, T. Watanabe, M. Hirano, H. Hosono, *J. Am. Chem. Soc.* 130 (2008) 3296.
- [2] Z. Ren, G. Che, X. Dong, J. Yang, W. Lu, W. Yi, X. Shen, Z. Li, L. Sun, F. Zhou, Z. Zhao, *EPL* 83 (2008) 17002.
- [3] F. Hunte, J. Jaroszynski, A. Gurevich, D. C. Larbalestier, R. Jin, A. S. Sefat, M. A. McGuire, B. C. Sales, D. K. Christen, D. Mandrus, *Nature* 453 (2008) 903.
- [4] F. Hsu, J. Luo, K. Yeh, T. Chen, T. Huang, P. Wu, Y. Lee, Y. Huang, Y. Chu, D. Yan, M. Wu, *Proc.Natl. Acad. Sci. U.S.A.* 105 (2008) 14262.

- [5] International Tables for Crystallography, Kluwer Acad. Publ. - Edited by T. Hahn, 1996.
- [6] M. H. Fang, H. M. Pham, B. Qian, T. J. Liu, E. K. Vehstedt, Y. Liu, L. Spinu, Z. Q. Mao, Phys. Rev. B 78 (2008) 224503.
- [7] K.-W. Yeh, T.-W. Huang, Y. lin Huang, T.-K. Chen, F.-C. Hsu, P. M. Wu, Y.-C. Lee, Y.-Y. Chu, C.-L. Chen, J.-Y. Luo, D.-C. Yan, M.-K. Wu, EPL (Europhysics Letters) 84 (2008) 37002.
- [8] Y. Mizuguchi, F. Tomioka, S. Tsuda, App. Phys. Lett. 94 (2009) 012503.
- [9] Y. Mizuguchi, F. Tomioka, S. Tsuda, J. Phys. Soc. Jpn. 78 (2009) 074712.
- [10] F. Nabeshima, Y. Kobayashi, Y. Imai, I. Tsukada, A. Maeda, Effect of co impurities on superconductivity of fese 0.4 te 0.6 single crystals, Japanese Journal of Applied Physics 51 (2012) 010102.
- [11] V. Bezusyy, D. Gawryluk, A. Malinowski, M. Berkowski, M. Cieplak, Acta Physica Polonica 126 (2014) A76.
- [12] J. Rodriguez-Carvajal, Physica B 192 (1993) 55.
- [13] R. A. Brand, Internat. Rep. Angewandte Physik, University of Duisburg, 1987.
- [14] K. Szymański, W. Olszewski, L. Dobrzyński, D. Satúa, D. J. Gawryluk, M. Berkowski, R. Puźniak, A. Wiśniewski, Supercond. Sci. Technol. 24 (2011) 105010.

- [15] R. W. Gómez, V. Marquina, J. L. Pérez-Mazariego, R. Escamilla, R. Escudero, M. Quintana, J. J. Hernández-Gómez, R. Ridaura, M. L. Marquina, *J. Supercond. Nov. Magn.* 23 (2010) 551.
- [16] A. Martinelli, A. Palenzona, M. Tropeano, C. Ferdeghini, M. Putti, M. R. Cimberle, T. D. Nguyen, M. Affronte, C. Ritter, *Phys. Rev. B* 81 (2010) 094115.
- [17] G. Garbarino, A. Sow, P. Lejay, A. Sulpice, P. Toulemonde, M. Mezouar, M. Núñez Regueiro, *EPL* 86 (2009) 27001.
- [18] N. C. Gresty, Y. Takabayashi, A. Y. Ganin, M. T. McDonald, J. B. Claridge, D. Giap, Y. Mizuguchi, Y. Takano, T. Kagayama, Y. Ohishi, M. Takata, M. J. Rosseinsky, S. Margadonna, K. Prassides, *Journal of the American Chemical Society* 131 (2009) 16944–16952.
- [19] M. Tegel, C. Löhnert, D. Johrendt, *Solid State Communications* 150 (2010) 383 – 385.
- [20] M. Bendele, P. Babkevich, S. Katrych, S. N. Gvasaliya, E. Pomjakushina, K. Conder, B. Roessli, A. T. Boothroyd, R. Khasanov, H. Keller, *Phys. Rev. B* 82 (2010) 212504.
- [21] F. Walz, *J. Phys. Condens. Matter.* 14 (2002) R285.
- [22] H. N. Ok, S. W. Lee, *Phys. Rev. B* 8 (1973) 4267–4269.
- [23] C. S. Yadav, P. L. Paulose, *J. Appl. Phys.* 107 (2010) 083908.
- [24] T. Kamimura, *J. Phys. Soc. Jpn.* 43 (1977) 1594.

- [25] N. Guigue-Millot, N. Keller, P. Perriat, *Phys. Rev. B* 64 (2001) 012402.
- [26] A. Wittlin, P. Aleshkevych, H. Przybyliska, D. J. Gawryluk, P. Dzewski, M. Berkowski, R. Puniak, M. U. Gutowska, A. Winiewski, *Superconductor Science and Technology* 25 (2012) 065019.
- [27] G. F. Goya, T. S. Berquó, F. C. Fonseca, M. P. Morales, *J. Appl. Phys.* 94 (2003) 3520.
- [28] Y. Mizuguchi, Y. Takano, *Journal of the Physical Society of Japan* 79 (2010) 102001.
- [29] X. Deng, J. Mravlje, R. Žitko, M. Ferrero, G. Kotliar, A. Georges, *Phys. Rev. Lett.* 110 (2013) 086401.
- [30] N. E. Hussey, K. Takenaka, H. Takagi, *Philosophical Magazine* 84 (27) (2004) 2847.
- [31] T. S. Su, Y. W. Yin, M. L. Teng, Z. Z. Gong, M. J. Zhang, X. G. Li, *Journal of Applied Physics* 114 (2013) 183901.
- [32] B. I. Shklovskii, A. L. Efros, *Electronic properties of doped semiconductors*, Springer-Verlag, 1984.
- [33] M. Tegel, C. Löhnert, D. Johrendt, *Solid State Comm.* 150 (2010) 383.
- [34] V. Tsurkan, J. Deisenhofer, A. Günther, C. Kant, M. Klemm, H. A. Krug von Nidda, F. Schrettle, A. Loidl, *Eur. Phys. J. B.* 79 (2010) 289.
- [35] R. Hu, E. S. Bozin, J. B. Warren, C. Petrovic, *Phys. Rev. B* 80 (2009) 214514.

- [36] T. J. L. et al., *Nature Materials* 9 (2010) 718.
- [37] G. Kotliar, A. Kapitulnik, *Phys. Rev. B* 33 (1986) 3146.
- [38] C. Tarantini, A. Gurevich, J. Jaroszynski, F. Balakirev, E. Bellingeri, I. Pallecchi, C. Ferdeghini, B. Shen, H. H. Wen, D. C. Larbalestier, *Phys. Rev. B* 84 (2011) 184522.
- [39] J. Kumar, S. Auluck, P. K. Ahluwalia, V. P. S. Awana, *Supercond. Sci. Technol.* 25 (2012) 095002.